Nuclear Engineering and Technology 53 (2021) 3398–3405

Contents lists available at ScienceDirect

Nuclear Engineering and Technology

journal homepage: www.elsevier.com/locate/net

Original Article

Influence of neutron irradiation and ageing on behavior of SAV-1 reactor alloy

K.V. Tsay [a, b], O.V. Rofman [a, *], V.V. Kudryashov [a, c], A.V. Yarovchuk [a], O.P. Maksimkin [a, d]

[a] Institute of Nuclear Physics, Almaty, 050032, Kazakhstan
[b] Al-Farabi Kazakh National University, Almaty, 050060, Kazakhstan
[c] Nazarbayev University, Nur-Sultan, 010000, Kazakhstan
[d] National Research Nuclear University MEPhI, Moscow, 115409, Russian Federation

ARTICLE INFO

Article history:
Received 23 September 2020
Received in revised form
10 February 2021
Accepted 26 April 2021
Available online 3 May 2021

Keywords:
SAV-1 aluminum alloy
Neutron irradiation
Fluence
Ageing
Precipitate
Corrosion

ABSTRACT

This study observed the effect of neutron irradiation and ageing on the microstructure, hardness, and corrosion resistance of SAV-1 (Al–Mg–Si) alloy. The investigated material was irradiated with neutrons to fluences of 10^{21}–10^{26} n/m^2 in the WWR-K research reactor and kept in dry storage. Long-term irradiation led to an increase in hardness of the alloy and a deterioration of pitting corrosion resistance. Post-irradiation ageing for 1 h at 100–300 °C resulted in a decrease in microhardness of the irradiated SAV-1. The effect of post-irradiation ageing on pitting corrosion was made clear through the formation of Guinier-Preston zones and secondary precipitates in the Al matrix. Ageing at 250 °C corresponded to the development of stable microstructure and the highest corrosion resistance for the irradiated samples. Mg_2Si, Si, and needle-shaped β″ precipitates were formed in SAV-1 alloy that was irradiated with low fluences. β″ and clusters of rod-shaped B-type precipitates were observed in highly irradiated samples. The precipitates were similar to those seen in non-irradiated pseudo-binary Al–Mg_2Si alloys with Si excess.

1. Introduction

Aluminum-based alloys that contain silicon have found applications in reactor engineering due to their completive nuclear-physical properties, including high ductility, thermal conductivity, and satisfactory resistance to water corrosion. Alloys of the Al–Mg–Si system (SAV, PAR) and their close analogues (6061 and 6063 alloys) are used in the structural elements of the core, as well as in the cooling and control systems of research nuclear reactors [1,2]. In the WWR-K reactor (Almaty, Kazakhstan), low-alloyed SAV-1 alloy is used in a hardened and naturally aged state to fabricate the protective ducts for fuel elements and automatic control rods (AC-rods) as well as in-vessel channels, shrouds and pipelines.

Aluminum materials are exposed to ultra-high neutron fluences (~10^{25}–10^{26} n/m^2) during long-term operation in the reactor core; significant changes in their microstructure and properties are therefore expected. A substantial increase in microhardness and yield strength values was seen in SAV-1 as well as other Al–Mg–Si alloys irradiated with neutrons or ions [3–9]. Possible reasons for alloys hardening under irradiation could include the growth of silicon content due to the Al (n, γ)Si nuclear reaction [1,6] and the formation of fine-sized Si and Mg_2Si precipitates. In addition, re-dissolution of primary Mg_2Si particles and the super-saturation of aluminum solid solution with Mg and Si components were considered as contributors for hardening [8].

Post-radiation effects also significantly influenced the properties of Al–Mg–Si alloys. The degradation of the structure due to radiation as well as variation in elemental and phase composition can negatively affect the resistance of reactor materials to corrosion [10]. These factors must be taken into account when determining optimal conditions for long-term post-radiation storage. The effect of ageing on properties of irradiated materials should also be evaluated. Ageing in non-irradiated Al–Mg–Si alloys, for example, takes place at elevated temperatures and leads to the formation of multiple intermetallic precipitates [11–17]. Neutron irradiation will likely generate numerous inhomogeneities, defects, and internal stresses that facilitate the formation of metastable phases in the alloys.

* Corresponding author.
E-mail address: o.rofman@inp.kz (O.V. Rofman).

https://doi.org/10.1016/j.net.2021.04.025

At present, there are limited numbers of studies on the influence of ageing on the structure and properties of Al–Mg–Si alloys irradiated with neutrons to high fluences [3,4,9]. It is a complex task to give a confident prediction as to the behavior and properties of irradiated Al–Mg–Si alloys at elevated temperatures. Therefore, the study focuses on microstructural changes in the SAV-1 alloy after neutron irradiation, storage, and post-irradiation ageing to expand knowledge on this subject. Transmission electron microscopy (TEM) and the X-ray energy dispersive spectroscopy (EDS) analysis were used to characterize the precipitates formed at different irradiation and post-irradiation conditions. Corrosion experiments were carried out using irradiated SAV-1 samples aged at different temperatures to evaluate the performance of the material in a severe water environment. The results obtained can be used to predict the behavior of ducts of spent fuel elements with unburnt nuclear fuel in case of a possible fault in storage conditions and an increase in temperature to 100–300 °C.

2. Materials and methods

The samples of SAV-1 alloy that conforms to GOST 4784-2019 standard (wt.%: balance Al, 0.5–0.6 Mg, 1.0–1.2 Si, ≤ 0.3Fe, 0.02 Ti, 0.01Cu, ≤ 0.03 Zn) were prepared from some regions of an AC-rod assembly irradiated with different fluences of neutrons. The assembly was composed of an AC-rod and a shank rod. The SAV-1 components of the assembly operated for a long time in the WWR-K reactor core and then kept in dry storage for about 20 years; therefore, it can be said that they were subjected to natural ageing. Sampling and irradiation conditions are presented in Fig. 1a. Alloy fragments were cut out from the top and bottom ends of the AC-rod duct (Fig. 1b) and the shank-rod (Fig. 1c) in the hot cell (Fig. 1d). Non–irradiated samples were used for comparative analysis and reference.

To study the effect of ageing on microstructure and properties of irradiated SAV-1 alloy, consecutive isochronous annealing was carried out for 1 h over the temperature range of 100–300 °C. Annealing of the specimens in a vacuum (< 6.7×10^{-3} Pa) was performed using a Nabertherm RD 30/200/11 electric furnace. The Vickers microhardness of the SAV-1 samples was measured before and after annealing using a PMT-3 microhardness tester (LOMO, Russian Federation) under applied loads on indenter of 50 g for the most hardened samples B and 20 g for other less hardened samples.

Structural TEM examinations of irradiated and aged samples were carried out both before and after annealing using a JEM-2100 transmission electron microscope (JEOL) equipped with an X-Max EDS detector (Oxford Instruments) at an accelerating voltage of 200 kV. TEM objects of SAV-1 samples after irradiation (before annealing) in the shape of 3 mm disks were thinned by a jet electropolishing in the electrolyte of 20 ml $HClO_4$ + 70 ml C_2H_5OH + 10 ml $C_3H_8O_3$. TEM bar-shaped samples ($2.8 \times 0.5 \times 0.1$ mm^3) of the SAV-1 after annealing were thinned by an argon ion beam in an Ion Slicer 09100IS (JEOL) to obtain a material thickness of ~0.1 μm.

Bars of 6 mm × 10 mm size and a minimum 1.5–2 mm in thickness were cut from the shank rod material (samples C and D) for corrosion studies. For comparison, samples of identical size were prepared from a non-irradiated SAV-1 alloy. The bars cut from the duct materials (A and B) were thin (less than 1 mm) and did not satisfy the size limits for the corrosion tests. The experiments on the corrosion resistance of the SAV-1 were carried out by immersing alloy samples in the 1% $FeCl_3$ solution for regular time intervals (2 h) at room temperature. $FeCl_3$ water solution was selected due to its similarity to the chemical parameters of the water in the pool-storage of the WWR-K reactor (Fe^{+3}: 0.1–0.8 mg/l; Cl^{+}: 0.01–0.1 mg/l and Al: 0.01–0.1 mg/l). The samples were periodically removed from the solution and then weighed using the KERN-770 electronic balance to determine any weight loss.

3. Results and discussion

3.1. Microstructure characterization

The initial state of the heat-treatable SAV-1 alloy before irradiation was as follows: heating to 520°C with subsequent quenching (for hardening) and natural ageing. The initial microstructure of the SAV-1 alloy was characterized by the segregation of Mg_2Si and Si large particles at the late stages of natural ageing. Data from EDS analysis collected from a non-irradiated SAV-1 sample after long-term storage at 20 °C is given in Fig. 2. EDS analysis showed the presence of globular particles of Si (spectrum 1), Mg_2Si (spectrum 2), and nano-precipitates (20–40 nm) enriched with Fe and Si (spectrum 3). The regions near large particles were depleted with Mg and Si. Grains of the initial SAV-1 alloy had a network dislocation structure with a density of ~ (2–4) × 10^{14} m^{-2}.

The microstructure of sample A irradiated to low doses is visually quite similar to a non-irradiated one (Fig. 3a). EDS analysis

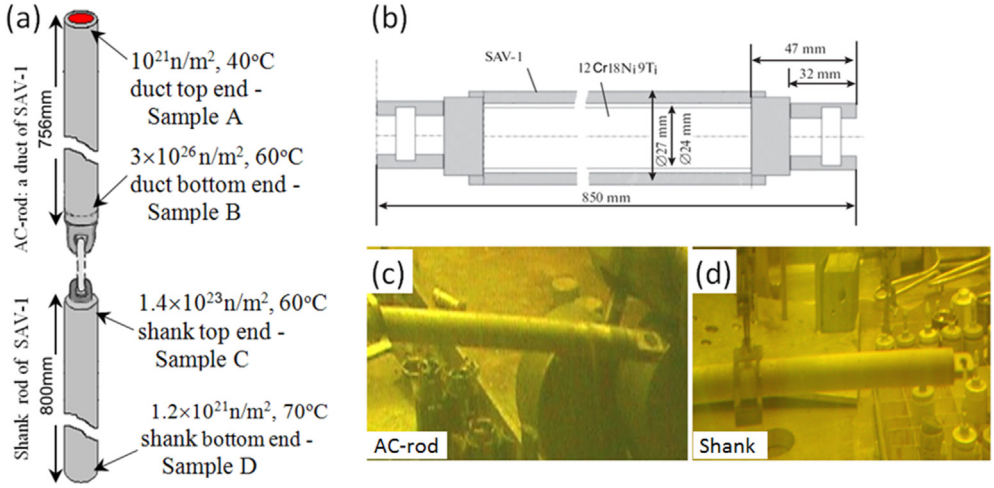

Fig. 1. Schematics of the AC-rod assembly in the reactor channel (a), the AC-rod drawing (b), and photos of the AC-rod (c) and the shank (d) in the hot cell before cutting. Samples A, B, C, D each refer to a set of samples cut from each point of interest.

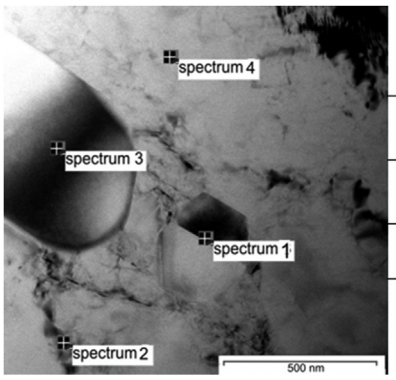

Spectrum	Elemental composition, wt.%				
	Mg	Al	Si	Fe	Total
1	0.1	2.7	97.2	-	100
2	0.8	92.4	2.5	4.3	100
3	62.8	-	37.2	-	100
4	-	99.8	0.2	-	100

Fig. 2. STEM electron image of non-irradiated SAV-1 alloy after natural ageing and the EDS data.

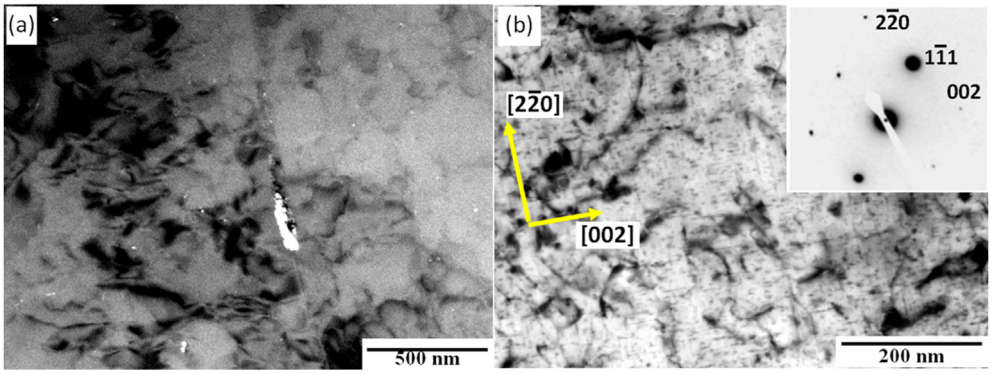

Fig. 3. (a) Dark field TEM image of Si precipitates (white area) in the sample A after irradiation and natural ageing. (b) Cluster defects and GP zones in the sample B after irradiation and natural ageing. Side image shows SAED from the specified area.

of the specimen showed the presence of Si nano-precipitates at the grain boundaries and dislocations. An extremely small quantity of Mg atoms was recorded near the silicon precipitates. The microstructure of the highly irradiated samples B contained a dislocation network and "ageing traces" (Fig. 3b) in shape of thin lined Guinier-Preston (GP) zones and clusters of 2–10 nm in size. In the aluminum matrix, GP lines with a length of up to 50 nm were arranged along the directions [2$\bar{2}$0] and [002]. Many grains were seen to have numerous cluster defects without GP zones. No additional fine-sized phases were observed in the sample B after irradiation and long-term storage.

Microstructures of the SAV-1 set of samples C and D after irradiation and storage were characterized by the presence of numerous defects in the form of perfect dislocation loops with sizes of 6–40 nm (Fig. 4). EDS scanning along a line crossing several loops was carried out. The EDS line profile of Si distribution revealed some small peaks which could be due to the positions of the loops. Dislocation loops in the SAV-1 alloy of the shank after irradiation and storage are apparently a result of the evolution of prismatic loops [14] formed by the collapse of vacancy clusters in the quenched initial SAV-1.

Artificial ageing of aluminum alloys may dramatically change their microstructure. For non-irradiated alloys, the sequence of ageing precipitates has been studied in detail in aged Al–Mg_2Si quasi-binary alloys with an excess presence of Si or Mg [14,15]. To reveal secondary precipitates which may present in neutron irradiated alloys, the SAV-1 samples were aged at 250 °C for 1 h and then examined by TEM.

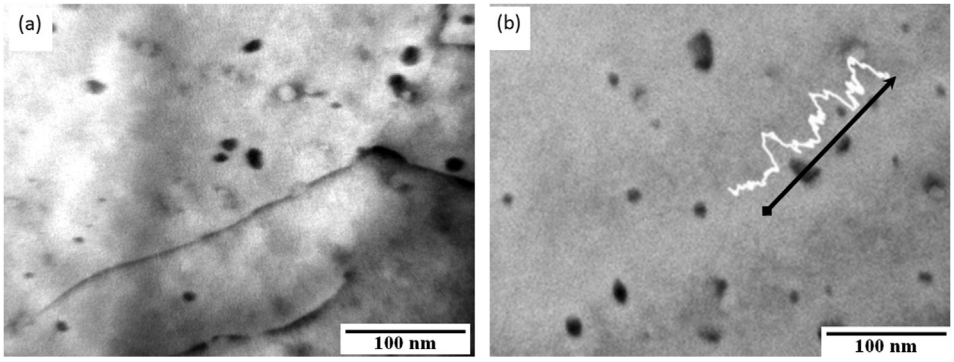

Fig. 4. Microstructure of the samples C (a) and D (b) after irradiation and natural ageing. The white graph represents EDS line scanning of Si.

After ageing at 250 °C, multiple precipitates of Si and plate-shaped cuboids β-Mg_2Si with the lattice parameter a = 0.639 nm [16] were observed in the microstructure of the weakly irradiated sample A (Fig. 5 a, b). The angle between $(111)_{Si}$ and $(110)_{Al}$ is five degrees. The SAED also showed the presence of needle-shaped β″-like precipitates in the aluminum matrix.

Needle-shaped precipitates were observed close to the monoclinic β″-phase with lattice parameters a = 1.516 nm, b = 0.405 nm, c = 0.674 nm, α = 105.3° [13] in the microstructure of the highly irradiated sample B after ageing (Fig. 5 c, d). Reflections in the microdiffraction pattern correspond to two orientations. For the β_1''phase, the orientation relationship is $(010)_{\beta''1} \parallel (0001)_{Al}$. The alloy microstructure also included a high-volume fraction of clusters of 3–10 nm in size as well as small rod-shaped precipitates.

The microstructures of the samples C and D after ageing are shown in Figs. 6 and 7. The β″and β-Mg_2Si precipitates were observed in the microstructure of the sample C aged at 250 °C. Additionally, rod-shaped precipitates with 5–30 nm width were observed. These rod-shaped precipitates are similar to those seen in the sample B (Fig. 5c). It follows from the SAED in Fig. 6b that a row of four reflexes most likely corresponds to the B-type metastable phase described in Ref. [12] in the Al–Mg_2Si alloy with Si excess aged at 250 °C. This phase has an orthorhombic lattice with parameters a = 0.684 nm, b = 0.793 nm, c = 0.405 nm. An angle between $[010]_P$ and $[010]_M$ equals 20°, and that is in line with [12] and confirms our conclusions.

Examination of the microstructure of the weakly irradiated sample D after ageing showed β″needles, Si and Mg_2Si precipitates. Fig. 7 shows the results of the EDS mapping of the aged sample D in a zone with a high concentration of precipitates. It was observed that most of the precipitates are silicon. A region depleted in silicon was formed locally in the grain due to the movement of silicon into the particles. From the EDS data it follows that the ageing precipitates (β″ needles) formed in this region of the matrix practically do not contain Si, but are actually enriched exclusively with Mg. A similar pattern was observed in the sample A (Fig. 5), where accumulations of silicon particles alternated with zones containing needles and rods precipitates.

3.2. Vickers microhardness measurements

Hardening of the SAV-1 alloy samples increased with an increase of fluence of neutrons. Fig. 8a shows the Vickers microhardness measured in irradiated SAV-1 samples before and after 1 h of annealing in the temperature range of 100–300 °C. Microhardness decreased steadily as the temperature increased for the samples A and B. The samples C and D had a local maximum of hardness at 200 °C. Microhardness values for samples A, C, and D aged at 250 °C were practically equal, but the one of the sample B was much higher. The concentration of ageing defects in the samples of A, C, and D is not very high and differs insignificantly, whereas the B sample contains a high density of ageing defects. Therefore, the maximum hardness is related to the amounts of cluster defects and β″needles in the sample.

The ageing products grow larger and partially re-dissolve in the aluminum matrix with an increase in the annealing temperature. As a result, the hardness of irradiated samples decreases sharply. The maximum rate of age softening was observed for the temperature range 250–300 °C and was typical for the sample B whereas the minimum rate was related to the non-irradiated sample. The rise of ageing time at 200 °C observed in Fig. 8b showed the increase in hardness of irradiated samples after 9 and again after 13 h

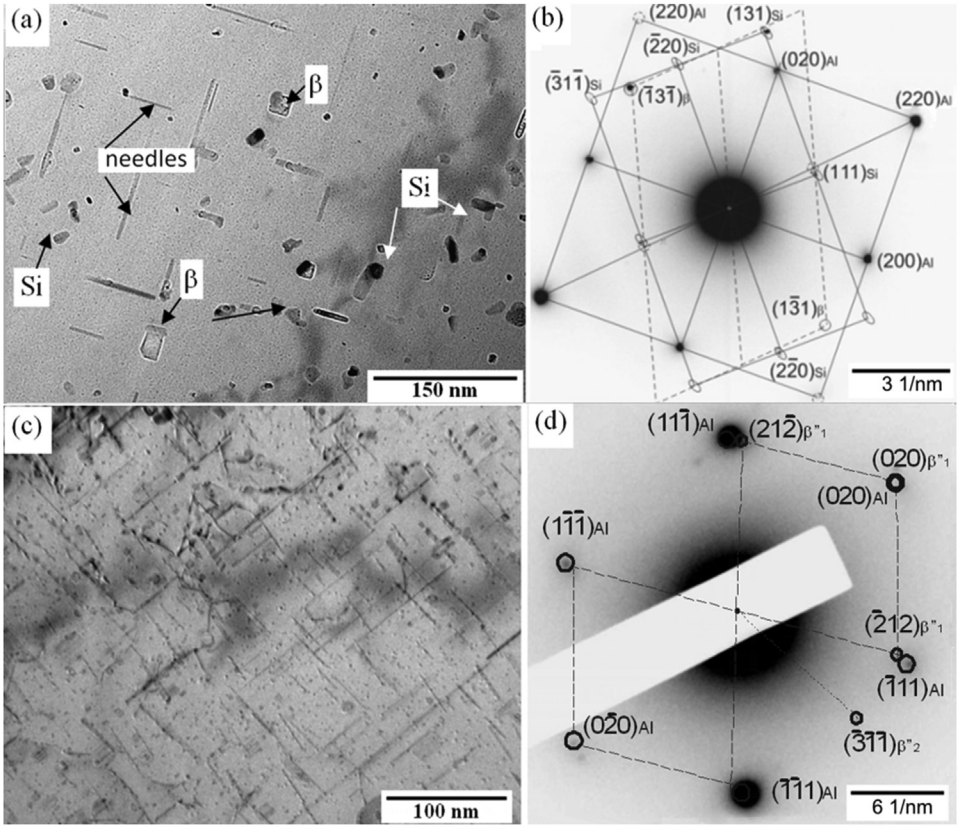

Fig. 5. Microstructure of the AC-rod duct samples after ageing at 250 °C for 1 h (a, b) Si-particles, cuboid β-Mg_2Si, and needle-shaped precipitates in the aged sample A. (c, d) Precipitates and cluster defects in the aged sample B. Bright field images (a, c) and microdiffraction patterns (b, d).

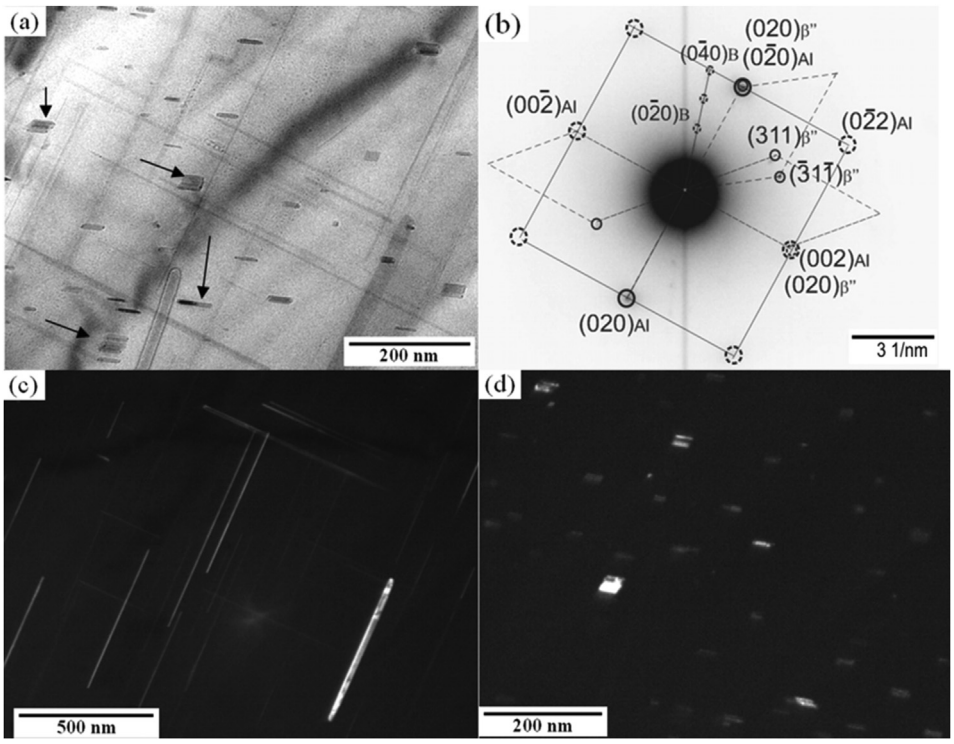

Fig. 6. Precipitates in the shank sample C aged at 250 °C for 1 h. (a) Bright-field TEM image; rod-shaped precipitates are indicated by arrows, (b) microdiffraction pattern, (c) dark-field image in (-31-1) of β″-phase, (d) dark-field image in (0-20) of B-Type phase.

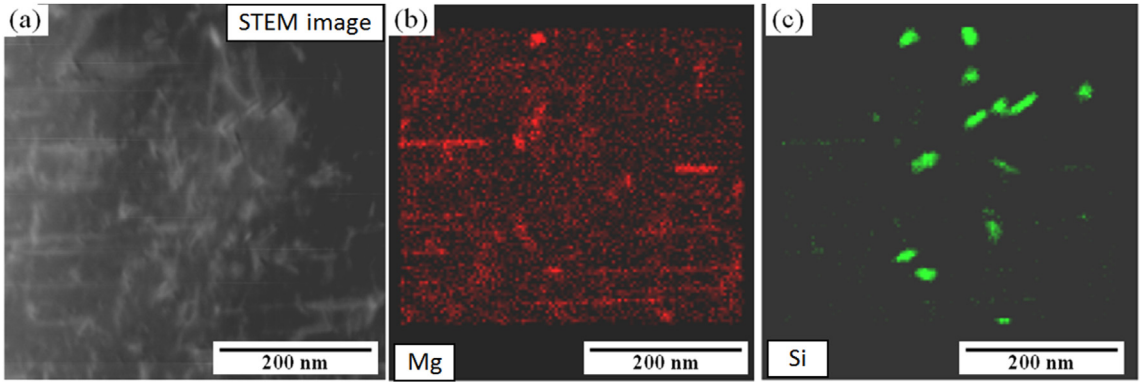

Fig. 7. EDS-mapping of the shank sample D after ageing at 250 °C for 1 h (a) STEM image; EDS results of mapping on Mg (b) and Si (c).

of exposure. This may be caused by ageing processes running in the material. However, such hardness increase was local and less than the total decrease in hardness as compared to irradiated alloys before annealing.

3.3. Corrosion tests

To study influence of ageing on the resistance to pitting corrosion, samples of the SAV-1 alloy both irradiated with neutrons and non-irradiated were tested in an environment containing chlorine. Fig. 9 shows the change in weight loss against time for SAV-1 samples subjected to corrosion by being immersed into a 0.1M$FeCl_3$ solution. Corrosion behavior of two samples irradiated to different fluences (C and D) and a non-irradiated one were compared. The weight losses of the samples showed a consistent increase with time of immersion. The lowest weight loss dependency was seen in a non-irradiated sample. During the first 50–60 h of the immersion test, the weight losses were reasonably consistent across all irradiated samples. It then follows that the higher irradiated sample C corroded more strongly than the lower irradiated sample D and that there was a quantitative difference in their weight losses.

Samples C were subjected to isochronous 1 h-annealings at different temperatures ranging from 150 to 250 °C. Comparative immersion tests on aged samples were conducted. The obtained dependencies of weight loss on immersion time for samples with different ageing temperatures are shown in Fig. 10a. It was shown that ageing samples became more resistant to corrosion. Here the corrosion rate after ageing at 200 °C became comparable with that of the more corrosion-resistant sample D (Fig. 9). Conversely, samples D after annealing at 150–200 °C showed a decrease in corrosion resistance (Fig. 10b).

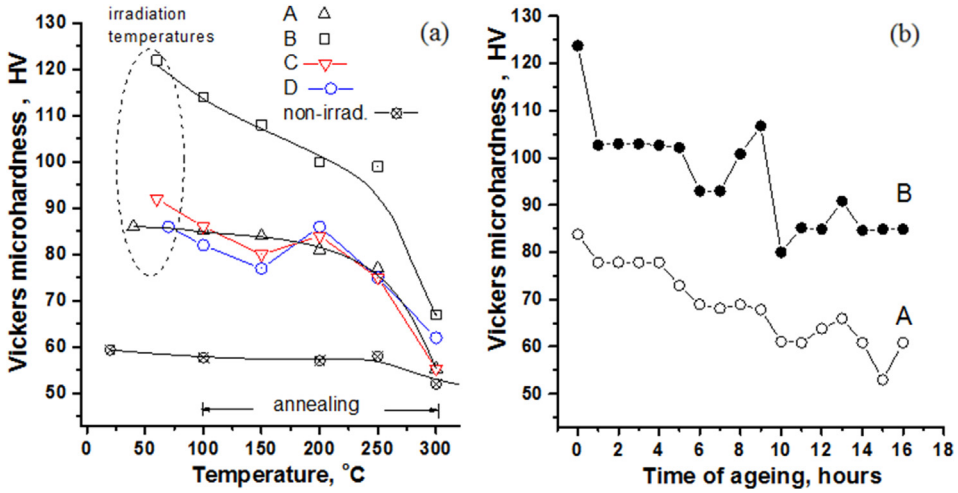

Fig. 8. (a) Change in the Vickers microhardness of SAV-1 alloy samples irradiated with neutrons and aged during 1-h annealing at different temperatures. (b) Change in the Vickers microhardness of the AC-rod duct samples A and B depending on time of ageing at 200 °C.

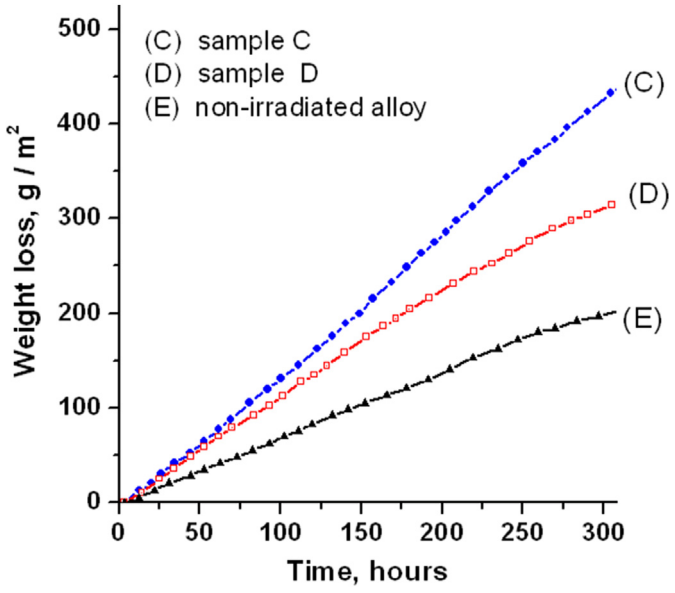

Fig. 9. Weight loss of the SAV-1 samples irradiated with neutrons against time of corrosion.

It is known that Mg_2Si formed by the natural ageing in Al–Mg–Si alloys reduce corrosion resistance. Mg_2Si inclusions are more cathodic than the matrix [18], however, they form a galvanic pair with aluminum, increasing the corrosion rate. Silicon particles are also cathodic than the matrix, but their effect on corrosion resistance is rather small because of the ultra-low density of the corrosion current [19]. Therefore, when the oxide film on the surface of the SAV-1 alloy is failed, pitting corrosion develops as the galvanic corrosion through erosion of the matrix around Mg_2Si particles.

The inhomogeneity and thermodynamic instability of the alloy structure subjected to long-term neutron irradiation have a significant effect on the corrosion resistance. The radiation-induced segregation (RIS) causes changes in the local composition of the alloy near the components of the structure – strong sinks of point defects (grain boundaries, dislocations, interphase boundaries etc.) [20]. As a result, new secondary inclusions were formed at the grain boundaries and in the matrix under irradiation. These phases were enriched with Mg and Si (Fig. 11), while the near-boundary regions could be depleted in alloying components. This increases the structural heterogeneity of the alloy and deteriorates its corrosion properties. In this case, the larger irradiation fluence is, the stronger the RIS effects are, which in turn reduce the corrosion resistance.

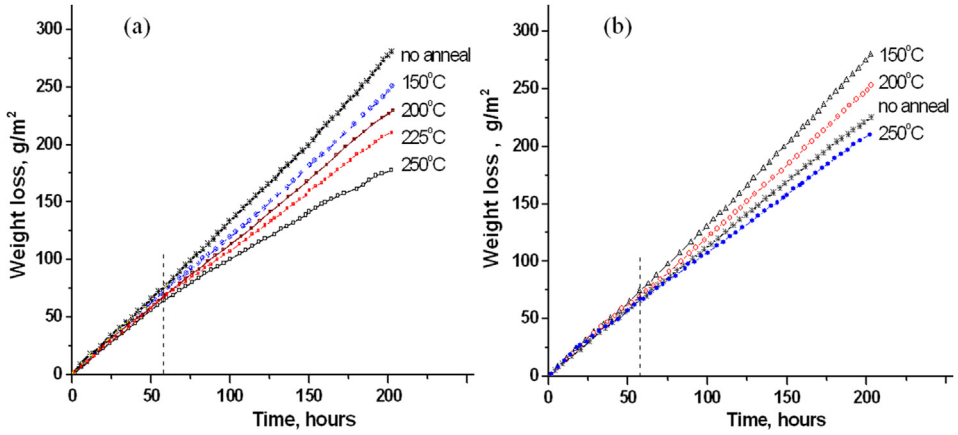

Fig. 10. Weight loss against corrosion time for samples C (a) and D (b) irradiated with neutrons and aged for 1 h at different temperatures.

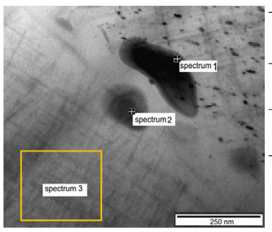

Spectrum	Elemental composition, wt.%			
	Mg	Al	Si	Total
1	2.98	94.34	2.68	100
2	2.22	92.15	5.63	100
3	0.63	98.78	0.59	100

Fig. 11. STEM electron image of secondary inclusions in the boundary region in the SAV-1 alloy irradiated with neutrons to 10^{21} n/cm^2 and 1 h-annealed at 200 °C.

Immersion tests on the irradiated SAV-1 samples annealed at temperatures of 150–200 °C showed that the corrosion resistances of highly and weakly irradiated alloys had reversed after ageing. The reason can be associated with the effect of several microstructural factors. The first factor is the preliminary radiation damage of SAV-1 alloy at temperatures <100 °C, leading to the creation of a thermodynamically nonequilibrium structure with a high level of internal stresses. The density of radiation defects, structural heterogeneity, and the level of internal stresses are higher in the alloy irradiated with a high fluence of neutrons (and the corrosion resistance, respectively, is lower) compared to the weakly irradiated one. The second factor is the poor solubility of magnesium silicide in the aluminum matrix. There are areas of nonequilibrium enrichment in Mg and Si in a non-irradiated alloy preserved after hardening. Heating the alloy at temperatures up to 200 °C leads to the formation of needle-like GP zones in the matrix which upon further heating (or with an increase in the heating duration) turn into a needle-shaped β″ phase and then into rod-like precipitates and finally to the plate-shaped equilibrium β phase (Mg_2Si) [13]. Ageing of the irradiated alloy samples at 200 °C also leads to the formation of GP zones in the microstructure. (Fig. 12). As a result of ageing, a partial relaxation of the internal stresses occurs in the structure of the highly irradiated alloy accompanied by the formation of a homogeneous network of GP zones, and the corrosion resistance increased. In the case of the weakly irradiated alloy, its structure became more inhomogeneous after ageing, new secondary precipitates of Mg2Si formed in the matrix and could worsen the corrosion resistance. The ageing temperature of 250 °C in both types of samples (C, D) corresponded to the most stable microstructure of the alloy considered. Here, the formation of thermodynamically equilibrium particles of Mg_2Si and Si, and no GP-zones were observed. In this case, the corrosion resistance increased in both types of samples compared to the state before annealing.

4. Conclusions

Changes in microstructure, hardness, and corrosion resistance of the SAV-1 aluminum alloy after irradiation with high fluences of neutrons ($10^{21} - 10^{26}$ n/m^2) and storage (natural ageing), as well as after 1 h-ageing over the temperature range 100–300 °C were discussed. The following conclusions were made:

(1) The alloy microstructure formed under irradiation gave rise to radiation hardening that increased with fluence increase. It can be caused by the appearance of pre-precipitates (clusters and GP zones) or by structure defects such as dislocation loops.
(2) Post-irradiation annealing of the irradiated SAV-1 samples led to a decrease in the hardness of the material, despite the possible ageing hardening seen in aluminum alloys. The maximal decrease in hardness corresponded to the temperature range of 250–300 °C.
(3) Ageing the irradiated SAV-1 alloy at 250 °C for 1 h generates a number of metastable intermetallic precipitates in the Al-matrix similar to ones in non-irradiated quasi-binary Al-Mg_2Si alloys with Si excess. Mg_2Si, Si, and needle-shaped β″ precipitates were observed in weakly (10^{21} n/m^2) irradiated SAV-1 alloys, and needle-shaped β″and rod-shaped B-type precipitates with cluster defects were observed in highly (10^{26} n/m^2) irradiated ones. The accumulation of silicon precipitates results in the depletion of the adjacent matrix in silicon and an enrichment in magnesium. This can change the ratio of Si and Mg atoms in the intermetallic precipitates, which is characteristic for a non-irradiated aluminum alloy.
(4) The formation of metastable microstructures in the SAV-1 alloy during irradiation, natural ageing, and post-irradiation ageing changes its resistance to pitting corrosion. The corrosion rate rises as irradiation fluence increases. The primary reason for the worsening of corrosion resistance is the inhomogeneity and thermodynamic instability of the structures after exposure to the high radiation dose. Post-radiation annealing leads to improvement of corrosion resistance in cases of higher neutron fluence and, conversely, to worsening of corrosion resistance for the material with a lower fluence. The results obtained show the need for a comprehensive account of the effect of GP-zones and new secondary precipitates on the corrosion resistance.

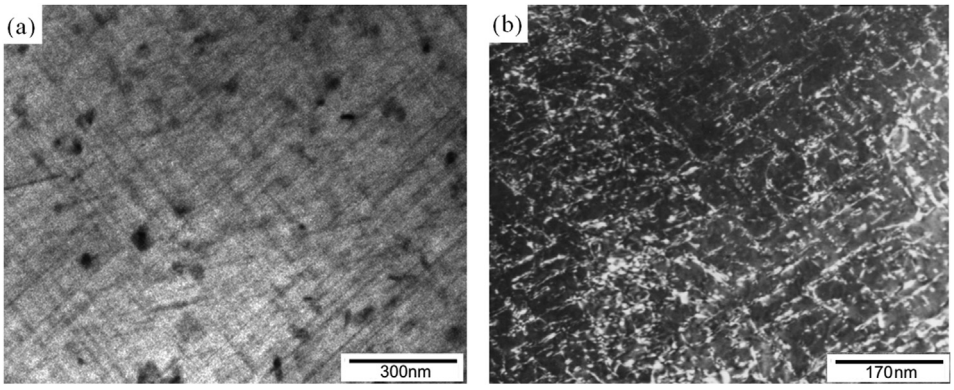

Fig. 12. The GP zones and secondary particles in the SAV-1 alloy after neutron irradiation and ageing at 200 °C (1 h) for the samples irradiated to 10^{21}n/cm^2 (a), and to 10^{26}n/cm^2 (b).

Declaration of competing interest

The authors declare that they have no known competing financial interests or personal relationships that could have appeared to influence the work reported in this paper.

Acknowledgements

This work was supported by the Grant No. BR09158499 of the Ministry of Energy of the Republic of Kazakhstan. The authors are grateful to Maxim Otstavnov, Nadezhda Sil'nyagina and Dr. Diana Merezhko for their assistance in preparation of this manuscript.

References

[1] A. Hoffman, A.Yu Didyk, A. Shteke, E.Khaevska, T.Wagner, V.K. Semina Effect of Nuclear Reactions on the Properties of Al-Mg-Si Alloys after Long-Time Exploitation in Research Reactors Communication of the JINR (Dubna) No P14-2004-174, 10 p.
[2] Renewal of the Reactor WWR-K Operation, Collection of articles [In Russian], IAE NNC RK, 1998, p. 248.
[3] Aluminium Taschenbuch, Verlag GmbH& Co, in: H. Nielsen, W. Hufnagel, G. Ganoulis (Eds.), Aluminium, Metallurgiya, Moscow, 1979 in Russian, Düsseldorf, 1974, p. 1056p.
[4] E.Z. Sturken, Irradiation effects in magnesium and aluminum alloys, J. Nucl. Mater. 82 (1979) 39–53.
[5] Z.E. Ostrovsky, G.A. Sernyaev, P.P. Grinchuk, S.N. Votinov, V. I, Prokhorov the effect of neutron irradiation on second phase precipitation processes, Transactions ISIJ 11 (1971) 289–293.
[6] V.M. Lebedev, V.T. Lebedev, I.N. Ivanova, S.P. Orlov, Structure of aluminum alloys irradiated with reactor neutrons, Phys. Solid State 52 (2010) 996–999.
[7] V.M. Lebedev, V.T. Lebedev, S.P. Orlov, B.Z. Margolin, A.M. Morozov, Small-angle neutron scattering investigation of the nanostructure of the SAV-1 alloy irradiated with fast neutrons to high fluences, Phys. Solid State 56 (2014) 161–165.
[8] D. Ueyama, Y. Saitoh, F. Hori, Y. Kaneno, K. Nishida, K. Dohi, N. Soneda, S. Semboshi, A. Iwase, Effects of energetic heavy ion irradiation on hardness of Al–Mg–Si alloys, Nucl. Instrum. Methods Phys. Res. Sect. B Beam Interact. Mater. Atoms 3141 (2013) 107–111.
[9] U.S. Salikhbaev, S.A. Baitelesov, I.G. Khidirov, F.R. Kungurov, V.S. Saidov, V.N. Sandalov Reactor, Irradiation influence on microstructure and microhardness of SAV-1 and AMG-2 aluminum alloy, Altern. Energy. Ekol. In Russian 9 (2008) 105.
[10] O.P. Maksimkin, K.V. Tsai, O.V. Rofman, N.S. Sil'nyagina, Effect of neutron irradiation and postradiation annealing on the microstructure and properties of an Al–Mg–Si alloy, Phys. Met. Metallogr. 117 (2016) 955–961.
[11] O.P. Maksimkin, Corrosion of aluminium alloy SAV-1 and austenitic stainless steels 12Cr18Ni10Ti and 08Cr16Ni11Mo3 – core structural materials for WWR-K and BN-350 reactors. Safety Related Issues of Spent Nuclear Fuel Storage, 2007, pp. 267–279.
[12] K. Matsuda, S. Ikeno, T. Sato, A. Kamio, Classification of metastable phases in Al-Mg2Si alloys by HRTEM, Mater. Sci. Forum 217–222 (1996) 707–712.
[13] S.J. Andersen, H.W. Zandbergen, J. Jansen, C. Tráholt, U. Tundal, O. Reiso, The crystal structure of the β″ phase in Al –Mg- Si alloys, Acta Mater. 46 (No. 9) (1998) 3283–3298.
[14] L.H. Doan, K. Nakai, Yo Matsuura, S. Kobayashi, Ya Ohmori, Effects of Excess Mg and Si on the isothermal Ageing behaviours in the Al-Mg2Si alloys, Mater. Trans. 43 (N6) (2002) 1371–1380.
[15] G. Meyruey, V. Massardier, W. Lefebvre, M. Perez, Over-aging of an Al-Mg-Si alloy with silicon excess, Mater. Sci. Eng. 730 (2018) 92–105.
[16] Crystallography open database. www.crystallography.net.
[17] M.H. Jacobs, The structure of the metastable precipitates formed during ageing of an Al-Mg-Si alloy, Philos. Mag. A 26 (1972) 1–13.
[18] E. Ghali, Corrosion Resistance of Aluminum and Magnesium Alloys. Understanding, Performance and Testing, Wiley Publication. –, – USA, 2010, p. 719.
[19] J.G. Kaufman, E.L. Rooy, in: R. Baboian (Ed.), Corrosion Test and Standards, Application and Interpretation, second ed., ASM International, Materials Park, OH, 2005, pp. 1–8.
[20] V.A. Pechenkin, A.D. Chernova, V.L. Molodtsov, G.V. Lysiva, YuV. Konobeev, Change in the properties of structural materials under irradiation: role of radiation-induced segregation, Atom. Energy 116 (2014) 301–310.